



Contents lists available at ScienceDirect

Biomaterials

journal homepage: [www.elsevier.com/locate/biomaterials](http://www.elsevier.com/locate/biomaterials)

## Extracellular vesicle-guided *in situ* reprogramming of synovial macrophages for the treatment of rheumatoid arthritis

Hyosuk Kim<sup>a,1</sup>, Ji Hyun Back<sup>b,c,1</sup>, Geonhee Han<sup>a,d</sup>, Su Jin Lee<sup>c</sup>, Yae Eun Park<sup>c</sup>, Man Bock Gu<sup>b</sup>, Yoosoo Yang<sup>a</sup>, Ji Eun Lee<sup>c,\*\*</sup>, Sun Hwa Kim<sup>a,\*</sup>

<sup>a</sup> Medicinal Materials Research Center, Biomedical Research Institute, Korea Institute of Science and Technology, Seoul, 02792, Republic of Korea

<sup>b</sup> Department of Biotechnology, College of Life Sciences and Biotechnology, Korea University, Seoul, 02841, Republic of Korea

<sup>c</sup> Chemical & Biological integrative Research Center, Biomedical Research Institute, Korea Institute of Science and Technology, Seoul, 02792, Republic of Korea

<sup>d</sup> KU-KIST Graduate School of Converging Science and Technology, Korea University, Seoul, 02841, Republic of Korea

### ARTICLE INFO

#### Keywords:

Macrophage  
Rheumatoid arthritis  
Extracellular vesicle  
Reprogramming  
Inflammation

### ABSTRACT

Activation state of synovial macrophages is significantly correlated with disease activity and severity of rheumatoid arthritis (RA) and provides valuable clues for RA treatment. Classically activated M1 macrophages in inflamed synovial joints secrete high levels of pro-inflammatory cytokines and chemokines, resulting in bone erosion and cartilage degradation. Herein, we propose extracellular vesicle (EV)-guided *in situ* macrophage reprogramming toward anti-inflammatory M2 macrophages as a novel RA treatment modality based on the immunotherapeutic concept of reestablishing M1-M2 macrophage equilibrium in synovial tissue. M2 macrophage-derived EVs (M2-EVs) were able to convert activated M1 into reprogrammed M2 (RM2) macrophages with extremely high efficiency (>90%), producing a distinct protein expression pattern characteristic of anti-inflammatory M2 macrophages. In particular, M2-EVs were enriched for proteins known to be involved in the generation and migration of M2 macrophages as well as macrophage reprogramming factors, allowing for rapid and efficient driving of macrophage polarization toward M2 phenotype. After administration of M2-EVs into the joint of a collagen-induced arthritis mouse model, the synovial macrophage polarization was significantly shifted from M1 to M2 phenotype, a process that benefited greatly from the long residence time (>3 days) of M2-EVs in the joint. This superb *in situ* macrophage-reprogramming ability of EVs resulted in decreased joint swelling, arthritic index score and synovial inflammation, with corresponding reductions in bone erosion and articular cartilage damage and no systemic toxicity. The anti-RA effects of M2-EVs were comparable to those of the conventional disease-modifying antirheumatic drug, Methotrexate, which causes a range of toxic adverse effects, including gastrointestinal mucosal injury. Overall, our EV-guided reprogramming strategy for *in situ* tuning of macrophage responses holds great promise for the development of anti-inflammatory therapeutics for the treatment of various inflammatory diseases in addition to RA.

### 1. Introduction

Synovial macrophages, a type of resident immune cell in synovial tissue, play a crucial role in the pathogenesis of rheumatoid arthritis (RA). In particular, the presence of abundant activated macrophages in arthritic synovial tissue is directly related to disease severity and prognosis of RA [1]. Owing to their high plasticity and heterogeneity, macrophages can become polarized into M1 pro-inflammatory or M2

anti-inflammatory phenotypes depending on stimulation by signals from the surrounding microenvironment [2,3]. In the healthy joint, large numbers of macrophages remain relatively quiescent as alternatively activated (M2) macrophages, which produce anti-inflammatory cytokines such as transforming growth factor- $\beta$  (TGF- $\beta$ ), interleukin-10 (IL-10) and IL-13. In swollen inflamed synovial tissue, however, classically activated, termed M1-type, macrophages secrete pro-inflammatory cytokines such as tumor necrosis factor- $\alpha$  (TNF- $\alpha$ ), IL-6 and IL-1 $\beta$ ,

\* Corresponding author. Medicinal Materials Research Center, Biomedical Research Institute, Korea Institute of Science and Technology, Seoul, Republic of Korea.

\*\* Corresponding author. Chemical & Biological integrative Research Center, Biomedical Research Institute, Korea Institute of Science and Technology, Seoul, Republic of Korea.

E-mail addresses: [jelee9137@kist.re.kr](mailto:jelee9137@kist.re.kr) (J.E. Lee), [sunkim@kist.re.kr](mailto:sunkim@kist.re.kr) (S.H. Kim).

<sup>1</sup> These authors contributed equally to this work.

<https://doi.org/10.1016/j.biomaterials.2022.121578>

Received 29 December 2021; Received in revised form 2 May 2022; Accepted 11 May 2022

Available online 16 May 2022

0142-9612/© 2022 The Author(s). Published by Elsevier Ltd. This is an open access article under the CC BY-NC-ND license (<http://creativecommons.org/licenses/by-nc-nd/4.0/>).

resulting in tissue destruction and bone erosion [4,5]. Thus, maintaining a balance between M1 and M2 through dynamic switching is necessary for beneficial processes that promote RA remission.

Disease-modifying antirheumatic drugs (DMARDs), conventional synthetic small chemical drugs with anti-inflammatory function, are typically the first-line pharmaceutical treatment for RA and are commonly given by oral, subcutaneous and intramuscular routes [6]. Because synovial joints have a relatively avascular structure with a limited peripheral blood supply, these systemic administration routes lead to insufficient accumulation of drugs in the target tissues, and also cause severe systemic adverse reactions, such as renal/liver impairment, bone marrow toxicity and gastrointestinal complications [7]. Therefore, intra-articular injections of drugs can be a good alternative for improving bioavailability and reducing systemic exposure. However, intra-articular administration of DMARDs provides limited benefit owing to the lack of local retention, reflecting the short half-lives (<4 h) of small molecules in the joint through clearance via the synovial vasculature and rapid draining through the lymphatics [8]. Focusing on this point, recent approaches to arthritis treatment using nanoparticles or extracellular vesicles (EVs) have been made [9–11]. However, most of these recent studies on RA treatment focus on relieving symptoms such as increased collagen production or macrophage depletion through inhibition of inflammation [12–15]. Unfortunately, therapeutic approaches based on macrophage depletion interfere with the crucial immune surveillance role of these cells, leading to serious systemic complications with long-term treatment, such as infections, ulcers and hepatitis. In this respect, shifting synovial macrophages to M2 phenotype can be a promising alternative strategy for RA therapy that targets the macrophage polarization. Indeed, several studies have investigated macrophage repolarization strategies using engineered nanoparticles for the treatment of RA [16,17]. However, these nanoparticles require additional complex engineering processes, and in terms of biocompatibility, adverse side effects and overzealous immune responses still remain. In this study, we propose EV-guided *in situ* macrophage reprogramming as a novel therapeutic tool in RA for effectively driving the direct conversion of pro-inflammatory M1 into anti-inflammatory M2 macrophages in synovial tissue (Fig. 1).

EVs, which transport various bioactive substances and act as central

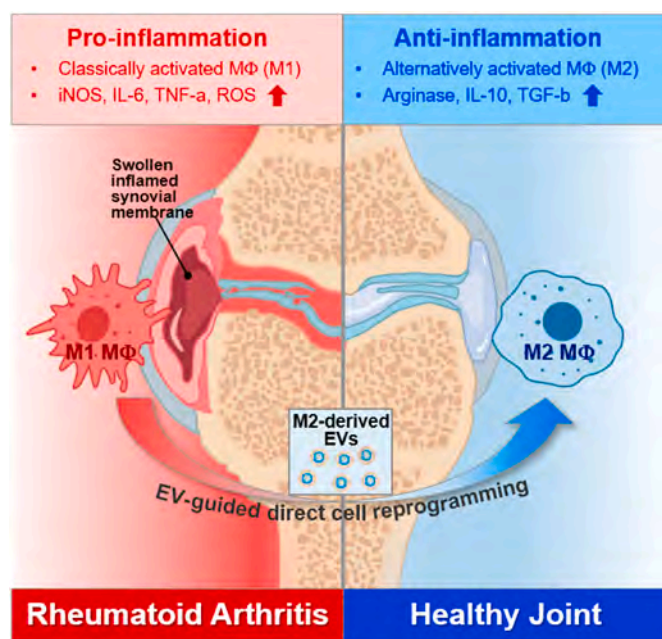


Fig. 1. Schematic illustration of the strategy for treating RA using M2 macrophage-derived extracellular vesicles (M2-EVs). M2-EVs could ameliorate RA by inducing the conversion of M1 into M2 macrophages.

mediators of intercellular communication, are emerging as promising therapeutic agents in a variety of diseases. Since the discovery that cell-derived EVs can induce phenotypic changes in recipient cells, many studies have explored the cargo content of EVs and their potential as cell-free therapeutics [18–20]. In addition to the function of EVs as carriers of bioactive molecules, the phospholipid-based envelopes of EVs make it easier for these vesicles to cross the plasma membranes of recipient cells, a critical step for successful local and systemic drug delivery. Herein, we found that M2 macrophage-derived EVs (M2-EVs) can rapidly and effectively reprogram M1 macrophages into functional M2-like macrophages *in vitro* and *in vivo*. The *in vitro* function of these reprogrammed M2 macrophages (RM2) derived from M1 phenotype was examined by evaluating their capacity to produce pro- and anti-inflammatory cytokines. RM2s displayed a protein expression pattern that was strikingly similar to that of M2 macrophages and were capable of producing high levels of anti-inflammatory cytokines together with significantly reduced secretion of pro-inflammatory cytokines. In-depth mass spectrometry-based proteomic analyses revealed that M2-EVs contained not only reprogramming factors that induce macrophage repolarization, such as glutamine synthase and milk fat globule-epidermal growth factor 8 (MFG-E8), but also anti-inflammatory factors such as matrix metalloproteinase 19 (MMP19) and chemokine (C–C motif) ligand 8 (CCL8). Unlike small chemical drugs with a very short joint half-life, M2-EVs had a long retention time of nearly 3 days within joints of collagen-induced arthritis (CIA) model mice, thus facilitating EV-guided *in situ* macrophage reprogramming toward anti-inflammatory M2 macrophages in the joint and ameliorating RA with no signs of systemic toxicity.

## 2. Material and methods

### 2.1. Preparation and culture of bone marrow-derived macrophages

Bone marrow-derived macrophages (BMDM) were prepared from DBA-1J mice as the previously described method [21]. First, the femur and tibia bones were separated from mice, and bone marrow was flushed into a 100 mm Petri dish using a 21 G needle with a 30 mL syringe in ice-cold Roswell Park Memorial Institute 1640 (RPMI 1640) media (Gibco). Bone marrow cells were cultured in RPMI 1640 media with 10% FBS (Gibco) containing 10 ng/mL of macrophage colony-stimulating factor (M-CSF) (Peprotech) for 7 days. On the 4th day of culture, additional media were added, and on the 6th day of culture, the media were changed. On the 7th day of culture, cytokines (Peprotech) for polarization of M1 and M2 macrophages were added and differentiated for 2 days (Fig. 2A, S1).

### 2.2. Separation and characterization of extracellular vesicles from BMDM

Separation of EVs from BMDM media was performed as previously described by Thery et al. [22] and reviewed by others [23]. The polarized macrophages were cultured in serum free media for 2 days, and the culture media were centrifuged at 300 g for 10 min (fixed angle JA-20 rotor, set at maximum acceleration and deceleration speed in Avanti J-E with Beckman Coulter) to separate remaining cells. Dead cells and cell debris were then removed by centrifugation at 2000 g for 10 min and 10,000 g for 30 min, respectively. The supernatant containing EVs was separated and centrifuged at 150,000 g for 90 min (fixed angle type 70 Ti rotor, set to maximum acceleration and deceleration speed on Optima XE-100 with Beckman Coulter). The EV pellet was washed once with PBS and then rotated again at 150,000 g for 90 min to pellet EVs. Finally, the EV pellet was re-suspended in the desired buffer, then aliquoted for storage at  $-80^{\circ}\text{C}$ .

For cryogenic transmission electron microscopy (Cryo-TEM) images of EVs, EV samples were fixed with 0.5% glutaraldehyde overnight. Then, the EV sample was centrifuged at 150,000 g for 30 min, re-

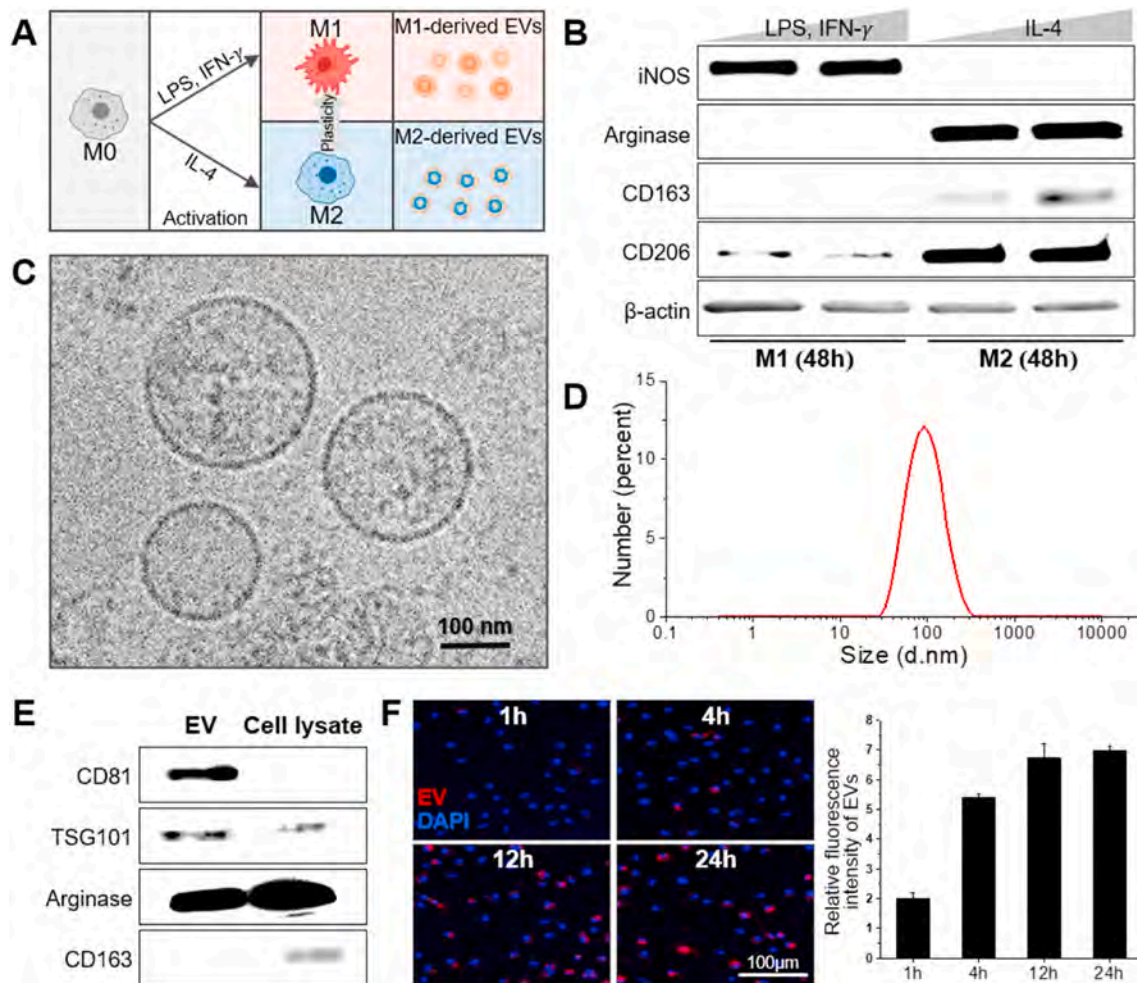


**Fig. 2.** Establishment of macrophage polarization and characterization of M2-EVs. (A) Schematic depiction of M1-EV and M2-EV preparation. (B) Western blot analysis showing differences in the expression of macrophage markers depending on the concentration of polarization factors. (C) Representative Cryo-TEM image of M2-EVs. (D) Size distributions of M2-EVs, analyzed by dynamic light scattering. (E) Immunoblotting for CD81, TSG101, arginase-1 and CD163 in M2-EVs and M2 macrophage lysates. (F) Confocal images and relative fluorescence intensity of M1 macrophages after incubating for 1, 4, 12 or 24 h with 100  $\mu$ g/mL of Cy5.5-N-hydroxysuccinimide (NHS ester)-labeled M2-EVs. Data are presented as means  $\pm$  SD ( $n = 6$ /group).

suspended with absolute ethanol and transferred to lacey carbon grid (Sigma-Aldrich). The grid was stored in liquid nitrogen and maintained at  $-180^{\circ}\text{C}$ . Images were taken with VitroBot<sup>TM</sup> (MARKII FP 5350/60, Thermo Fisher Scientific). EVs were quantified by bicinchoninic acid protein (BCA) assay (Thermo Fisher Scientific) and their size distributions were determined by dynamic light scattering analysis (Malvern Instruments). Immunoblotting was performed to identify EV markers CD81 (ab79559, Abcam; 1:200) and tumor susceptibility gene 101 protein (TSG101) (ab125011, Abcam; 1:200).

### 2.3. Labeling and cellular uptake of EVs

EVs were labeled by incubation with cyanine 5.5-N-hydroxysuccinimide ester (Cy5.5-NHS ester) for 3 min at  $37^{\circ}\text{C}$ . After incubation, unreacted Cy5.5-NHS ester was removed with a column (MWCO 3000 Da, Invitrogen). Cells including macrophages, T cells, dendritic cells and NIH-3T3 were seeded at density of  $3 \times 10^5$  cells in 35 mm confocal dish, incubated at  $37^{\circ}\text{C}$  with labeled EVs (100  $\mu$ g/mL) for 1, 4, 12 and 24 h, then observed with a confocal microscope (Leica TCS SP6, Germany). The fluorescence intensities were quantified using an image analyzer. EEA1 (Abcam, UK, ab206860, 1:200) was used for staining of early endosomal marker.

### 2.4. Western blot analysis

Total protein prepared in standard RIPA buffer (25 mM Tris-HCl, pH 7.6, 150 mM NaCl, 1% NP-40, 1% sodium deoxycholate and 0.1% SDS) was diluted with  $5 \times$  standard SDS loading buffer and heated at  $95^{\circ}\text{C}$  for 5 min. The equal amount of cell lysate protein (20  $\mu$ g) measured by BCA assay was separated with 10% sodium dodecyl sulfate polyacrylamide gel electrophoresis (SDS-PAGE) gel and transferred onto 0.45  $\mu$ m nitrocellulose membrane. Then, membranes were blocked for 30 min at room temperature in 5% skim milk and subsequently incubated with primary antibodies overnight at  $4^{\circ}\text{C}$ . Next day, the membranes were washed three times for 15 min with Tris Buffered Saline pH 7.5 with 0.1% Tween 20 (TBS-T) and incubated with horseradish peroxidase (HRP) tagged second antibodies in blocking solution for 1 h. The labeled proteins were visualized with LAS-3000 Luminescent Image Analyzer (FujiFilm). The antibodies used in this study were as follows: iNOS (ab210823, Abcam; 1:200), arginase-1 (#93668, CST; 1:200), CD163 (ab182422, Abcam; 1:200), CD206 (SC-376108, Santa Cruz Biotechnology; 1:200),  $\beta$ -actin (ab8227, Abcam; 1:1000), anti-mouse-HRP (ab6728, Abcam; 1:2000) and anti-rabbit-HRP (ab6721, Abcam; 1:2000).

## 2.5. Quantitative RT-PCR analysis and ELISA assay

Total RNA was extracted with TRIzol Reagent (Invitrogen) and complementary DNA templates were synthesized using the Superscript III First-Strand Synthesis System (Invitrogen). RT-qPCR was performed on StepOnePlus Real-Time PCR System (Applied Biosystems) by using SYBR Green PCR Master Mix (Applied Biosystems), with each sample prepared in triplicate according to the manufacturer's protocol. The expression data were normalized to GAPDH levels and assessed using  $\Delta\Delta C_t$  method. For ELISA assays, cell culture supernatants were collected by centrifugation at 1500g for 10 min at 4 °C to remove cell debris. Mouse M1/M2 Cytokines multiplex ELISA Kit (# ARG82913) were purchased from Arigobio (Hsinchu, Taiwan) and the expression of all cytokines was measured according to the manufacturer's instructions.

## 2.6. Proteomic analyses

M1, M2 and RM2 macrophages obtained from treatment of M2-EVs were lysed in RIPA buffer with protease inhibitor cocktail. EVs, respectively, derived from M1 and M2 macrophages were also lysed in RIPA buffer with protease inhibitor cocktail. The protein concentrations were determined using BCA assay and the proteins were separated based on molecular weight using 4–12% Bis-Tris gel. While 100 µg of each type of macrophage samples were run in triplicate on the same gel, 95 µg of each type of EV sample was run in duplicate on the same gel. After the gel was stained with Coomassie Brilliant Blue R-250, the stained gel for each lane of sample was divided into 14 slices and the proteins contained in each gel slice were subjected to trypsin digestion. Briefly, the proteins were reduced with 10 mM dithiothreitol in 25 mM  $\text{NH}_4\text{HCO}_3$  for 1 h at 56 °C and alkylated with 55 mM iodoacetamide in 25 mM  $\text{NH}_4\text{HCO}_3$  for 1 h at 25 °C in the dark followed by trypsin digestion overnight. Peptides were then extracted with 67% acetonitrile (ACN)/5% formic acid (FA) in water. The extracted peptides in each tube were dried in a SpeedVac and subsequently re-suspended with 20 µL of 0.4% acetic acid.

For mass spectral analysis, 13.5 µL of each sample was injected into a reversed-phase Magic C18AQ column (15 cm × 75 µm) on an Eksigent MDLC system (Eksigent Technologies Dublin). The operating flow rate was 350 nL/min, with the following gradient conditions: 0 min 100% buffer A (100% water with 0.1% formic acid) and 0% buffer B (100% acetonitrile with 0.1% formic acid), 0–5 min 0–8% B, 5–85 min 8–30% B, 85–90 min 30–70% B, 90–100 min 70% B, 100–110 min 70–2% B and 100–120 min 2% B. The nano HPLC system was coupled to an LTQ XL-Orbitrap mass spectrometer (Thermo Fisher Scientific). The spray voltage was set to 2.5 kV and the temperature of the heated capillary was set to 250 °C. Survey full-scan mass spectrometry (MS) spectra (300–1800  $m/z$ ) were acquired with 1 microscan at a resolution of 60,000, allowing preview mode for precursor selection and charge-state determination. Tandem mass (MS/MS) spectra for the ten most intense ions from the preview survey scan were acquired concurrently in the ion trap with the following options: isolation width, 2  $m/z$ ; normalized collision energy, 35%; dynamic exclusion duration, 360 s. Precursors with +1 charge and unassigned charge states were discarded during data-dependent acquisition. Each LC-MS/MS file was searched against the SwissProt mouse database (November 2020) with 17196 entries using Proteome Discoverer software (version 2.4, Thermo Fisher Scientific). The search criteria were set to a mass tolerance of 15 ppm for MS data and 0.5 Da for MS/MS data with fixed modification of carbamidomethylation of cysteine (+57.021 Da) and variable modification of methionine oxidation (+15.995 Da). The false discovery rate (FDR) was set at 0.01 for identification of peptides and proteins. All proteins were identified by two or more unique peptides.

The relative abundances of proteins, respectively, among M1, M2 and RM2 macrophages induced by M2-EVs and between M1-EVs and M2-EVs were calculated based on peak areas using Minora algorithm-based label-free quantification in Proteome Discoverer 2.4. Statistical

analysis of the dataset obtained from the label-free quantification was performed using Perseus software (1.6.14.0) [24]. Normalized abundance values obtained from peak area normalized by total peptides were log-transformed. Missing values were replaced using values computed from the normal distribution with a width of 0.3 and a downshift of 1.8. Proteins exhibiting statistical significances among M1, M2 and RM2 macrophages were detected by one-way analysis of variance (ANOVA) comparison of the  $\log_2$  (normalized abundance) values obtained from the three replicates of each type of macrophage samples. Statistically significant proteins between M1-EVs and M2-EVs were found by Student's *t*-test comparison of the  $\log_2$  (normalized abundance) values obtained from the two replicates of each type of EV samples. A *p*-value <0.05 was considered statistically significant. For hierarchical clustering of proteins showing statistically significant changes (>2.0-fold, *p*-value <0.05) in M2 and RM2 macrophages compared to M1 macrophage or between M1-EVs and M2-EVs, normalized abundance values were first normalized using z-score and then clustering of both columns and rows was pursued based on Euclidean distance using the average linkage method using Perseus (1.6.14.0). Gene Ontology (GO) functional classifications were analyzed with DAVID software (<http://david.abcc.ncifcrf.gov>). GO term over-representation analysis was performed to identify GO terms that were significantly enriched in either protein showing significant changes in M2 and RM2 macrophages in comparison to M1 macrophages or identified proteins from EV samples. STRING was used to visualize functional interaction network for the proteins specifically identified from M2-EVs with minimum required interaction score as medium confidence (0.4) [25].

## 2.7. In vivo biodistribution study of EVs

For the *in vivo* biodistribution test, mice received footpad injection of Cy5.5-labeled EVs (100 µg/20 µL) and PBS (*n* = 3). The whole-body fluorescence images were taken every 24 h after administration by the *in vivo* imaging system (IVIS) Lumina Series III (PerkinElmer). After 48 h of post-administration, major visceral organs (liver, lung, spleen, kidney and heart) and hind paws from treated mice were extracted and analyzed with IVIS Spectrum system. Quantification of fluorescence intensities in region of interest (ROIs) was analyzed using Living Image software (PerkinElmer).

## 2.8. In vivo therapeutic effects of EVs in murine collagen-induced arthritis (CIA) model

CIA animal model was prepared as previous described with minor modification [26]. Briefly, DBA/1J mice were injected intradermally at the base of the tail with 200 µg of bovine type II collagen (2 mg/mL, Chondrex) emulsified in 100 µL of complete Freund's adjuvant (4 mg/mL, Chondrex). On day 21, the booster immunization with incomplete Freund's adjuvant was induced. Since there was a limit to the injection volume of intra-articular EV administration due to the relatively small spatial structure of the mouse ankle joint, animal experiments were performed using the footpad injection method. Twenty-one days after the first immunization, PBS and M2-EVs (100 µg/20 µL) were injected into footpads of mice, and MTX (2.5 mg/kg) was injected intraperitoneally every 4 days. The hind limbs of CIA mice were clinically scored as follows: 0 = no sign of inflammation, 1 = mild inflammation with minimal hyperplasia of the synovial lining layer with cartilage destruction, 2 = mild swelling and erythema extending to the midfoot and ankle joint, 3 = moderate swelling and erythema extending from the metatarsal joints to the ankle and 4 = severe swelling and erythema encompassing the foot, ankle and digits. These paw scores were summed up to give maximum possible score of 16 per mouse [27]. All animal experiments were carefully performed in accordance with the International Guide for the Care and Use of Laboratory Animals and approved by Korea Institute of Science and Technology.

## 2.9. Hepatotoxic injury assay

For alanine aminotransferase (ALT) and aspartate aminotransferase (AST) tests, PBS, M2-EVs (100 µg/20 µL) and MTX (2.5 mg/kg) were injected into footpads of DBA/1J mice every 4 days. After 21 days, blood samples were collected via cardiac puncture and blood was allowed to clot at room temperature for approximately 10 min. The coagulated blood samples were centrifuged at 3000 rpm for 15 min at 4 °C to collect serum. AST and ALT kits were purchased from BioVision, and the activity of all serum enzymes was measured according to the manufacturer's instructions.

## 2.10. Histological analysis

After the therapeutic monitoring for 24 days, dissected arthritis joints were fixed in 10% buffered formalin, decalcified using Decalcified Solution-Lite (Sigma-Aldrich) for 6 h, embedded in paraffin and sliced into 5 µm-thick sections. Joint sections were stained with hematoxylin and eosin (H&E) and safranin O/fast green, and examined under an optical microscopy BX 51 Olympus (Olympus). For micro-computed tomography (micro-CT), the hind paws were harvested in saline and immediately stored at -80 °C. The cross-section images of hind paw specimens were acquired at an isotropic resolution of 35 µm a micro-CT system (Skyscan 1076, Skyscan). Scanning parameters were set as follow: 100 kV X-ray voltage, 100 µA current, 275 ms exposure time and 0.4° rotation steps with a 1-mm-thick aluminum filter. The terminal deoxynucleotidyl transferase dUTP nick end labeling (TUNEL) staining of the joint sections was carried out with DeadEnd™ Fluorometric TUNEL System (Promega) according to the manufacturer's instructions.

## 2.11. Flow cytometry analysis

To isolate synovial macrophages, the hind paw was dissected, and the skin, muscles and tendons were removed. After chopping the tissues, cells were dissociated by incubating with RPMI media containing 10% FBS, collagenase from *Clostridium histolyticum* (2 mg/mL, Sigma-Aldrich) and DNase (0.03 mg/mL, Sigma-Aldrich) for 45 min. For flow cytometry analysis, macrophages were fixed with 4% paraformaldehyde and permeabilized with 0.25% Triton X-100. Then, the fixed cells were incubated with primary antibodies in 5% BSA for 2 h at 4 °C. After two PBS washes, the cells were stained with secondary antibodies in the dark for 1 h at 4 °C. The stained macrophages were analyzed by flow cytometry (Guava easyCyte Flow Cytometers, MERCK). For *in situ* reprogramming analysis, the cells were labeled with Celltracker™ Green CMFDA (Thermo Fisher Scientific) according to the manufacturer's instructions. The antibodies used in this study were as follows: CD206 (SC-376108, Santa Cruz Biotechnology; 1:200), F4/80 (ab105155, Abcam; 1:200) Alexa Fluor 488 (ab150117, Abcam; 1:500) and Alexa Fluor 647 (ab150083, Abcam; 1:500).

## 2.12. Statistical analysis

All data was expressed as mean ± standard deviation (SD) and analyzed using a one-way analysis of variance (ANOVA) followed by Tukey's multiple comparison post-hoc test. A value of  $p < 0.05$  was considered statistically significant. Statistical significance is indicated as \*  $p < 0.05$ , \*\* $p < 0.01$  and \*\*\* $p < 0.001$ .

## 3. Results and discussion

### 3.1. Establishment of M1 and M2 macrophages and characterization of M2-EVs

To obtain a cell source of EVs for macrophage reprogramming, we first extracted bone marrow cells from femurs and tibias of DBA-1J mice, which are commonly used in CIA models, employing the method

described in a previous study [21]. The extracted bone marrow cells were differentiated into naïve M0 macrophages by culturing with monocyte-colony stimulating factor (Fig. 2A). Since several studies have reported differences in polarization methods and degree of polarization to M1 and M2 macrophages between mouse species [28,29], we investigated the extent of polarization as a function of the concentration of polarization factors and polarization time by Western blotting (Fig. S1 and 2B). Lipopolysaccharide (LPS)/interferon gamma (IFN-γ) and interleukin-4 (IL-4) were used to polarize M0 macrophages into pro-inflammatory M1 and anti-inflammatory M2 macrophages, respectively. Macrophages treated with 100 ng/mL of LPS expressed significantly lower levels of M2-specific marker CD206 and clearly expressed M1 marker iNOS at 24 h. In M2-polarized macrophages, expression of M2 marker CD163 was first detected within 24 h of treatment with IL-4 (20 ng/mL). After treatment with IL-4 for 48 h, expression levels of M2 markers arginase-1, macrophage scavenger receptor (CD163) and macrophage mannose receptor 1 (CD206) were significantly increased, confirming that the macrophages were completely polarized to M2 phenotype.

M2-EVs were harvested from M2 macrophage culture media using an ultracentrifugation method. The physicochemical properties of M2-EVs (size and shape) were examined by transmission electron microscopy (TEM) and dynamic light scattering (DLS) analysis (Fig. 2C and D). M2-EVs observed by Cryo-TEM exhibited a characteristic spherical shape with a lipid bilayer membrane and a size of ~100 nm, a value consistent with the Z-average particle diameter detected by DLS. In addition, the shape and size of these EVs were maintained at 37 °C for about 4 days and showed high stability. We then explored whether the general EV-specific markers, CD81 and tumor susceptibility gene 101 protein (TSG101), were expressed in M2-EVs using Western blot analysis (Fig. 2E). In addition to these EV-specific markers, M2-EVs also expressed the M2 macrophage marker, arginase-1, but did not express the highly specific M2-type macrophage marker, CD163. EVs are known to serve as intercellular messengers that carry cargoes such as nucleic acids, proteins and lipids from parent cells to other cells [30]. Thus, CD163 was selected as a marker for *in vitro* reprogramming experiments that could rule out the possibility of simple delivery of M2-specific markers via M2-EVs. It is known that the EV-uptake efficiency of myeloid cells differs depending on their differentiation status; in particular, macrophages have highly efficient cellular uptake mechanisms for EVs [31]. To examine the EV-uptake efficiency of M1 macrophages, we incubated M1 macrophages (100 µg/mL) with fluorescent dye-labeled EVs for 1, 4, 12 or 24 h (Fig. 2F). As expected, confocal microscopy images showed that a significant number of EVs were absorbed by macrophages within 4 h, and cellular uptake of EVs was saturated after 24 h. In order to further explore the targeting ability of EVs, the cellular uptake behaviors of EVs were investigated with different types of cells including macrophages, T cells, dendritic cells and fibroblasts (Fig. S2A). Interestingly, M2-EVs exhibited favorable cellular uptake in the macrophage group, suggesting the possibility that macrophage-originated EVs selectively target macrophages themselves. Several studies have already shown that EVs can recognize the parent cells and be taken up in a cell-specific manner [32–34]. It was also confirmed that M2-EVs were successfully internalized through endocytosis by observing the co-localization between early endosomal markers, EEA1 (Early Endosome Antigen 1), and EVs in cells (Fig. S2B).

### 3.2. M2-EVs induce effective *in vitro* reprogramming of M1 into fully functional M2 macrophages

Although the critical role of the immunomodulatory function of macrophages in RA therapy has been extensively studied [5,35,36], most previous studies have investigated one-way approaches for reducing the inflammatory response by simply depleting local/systemic pro-inflammatory macrophages or recruiting more anti-inflammatory macrophages from the circulation [37–41]. These systemic

macrophage-deletion strategies may disturb macrophage-mediated immune surveillance and cause unusual adverse reactions, including infections or hepatitis. In this regard, *in situ* reprogramming of tissue-resident macrophages from anti-inflammatory M1 to pro-inflammatory M2 phenotype could be an attractive therapeutic approach for RA. To induce EV-guided macrophage reprogramming toward M2 phenotype, we cultured classically activated M1 macrophages in serum-free media containing 100 µg/mL of M2-EVs (Fig. 3A). Immunocytochemical analyses performed after a 24 h incubation revealed that M2-EVs completely turned on the M2-marker arginase-1 and turned off the M1-marker iNOS in RM2 macrophages (Fig. 3B). In addition to causing a morphological change from round to elongated/dendritic shapes, M2-EVs significantly up-regulated the expression

of CD206 and CD163, major markers of M2 macrophages, in RM2 macrophages (Fig. 3C). The fact that M2-EVs do not carry CD163 indicates induction of RM2 reprogramming rather than a simple transfer of M2-specific proteins, reflecting the excellent macrophage-switching capability of M2-EVs. To further explore changes in the functional status of RM2 macrophages, we monitored the production of representative pro- and anti-inflammatory cytokines in M1, M2 and RM2 macrophages using quantitative reverse transcription-polymerase chain reaction (RT-qPCR) and ELISA assay (Fig. 3D and S3). As expected, expression levels of the pro-inflammatory cytokines TNF-α and IL-6 were low in RM2 macrophages and similar to levels found in M2 macrophages, whereas the production of anti-inflammatory cytokines such as TGF-β, IL-4 and IL-10 in these cells was significantly increased compared with

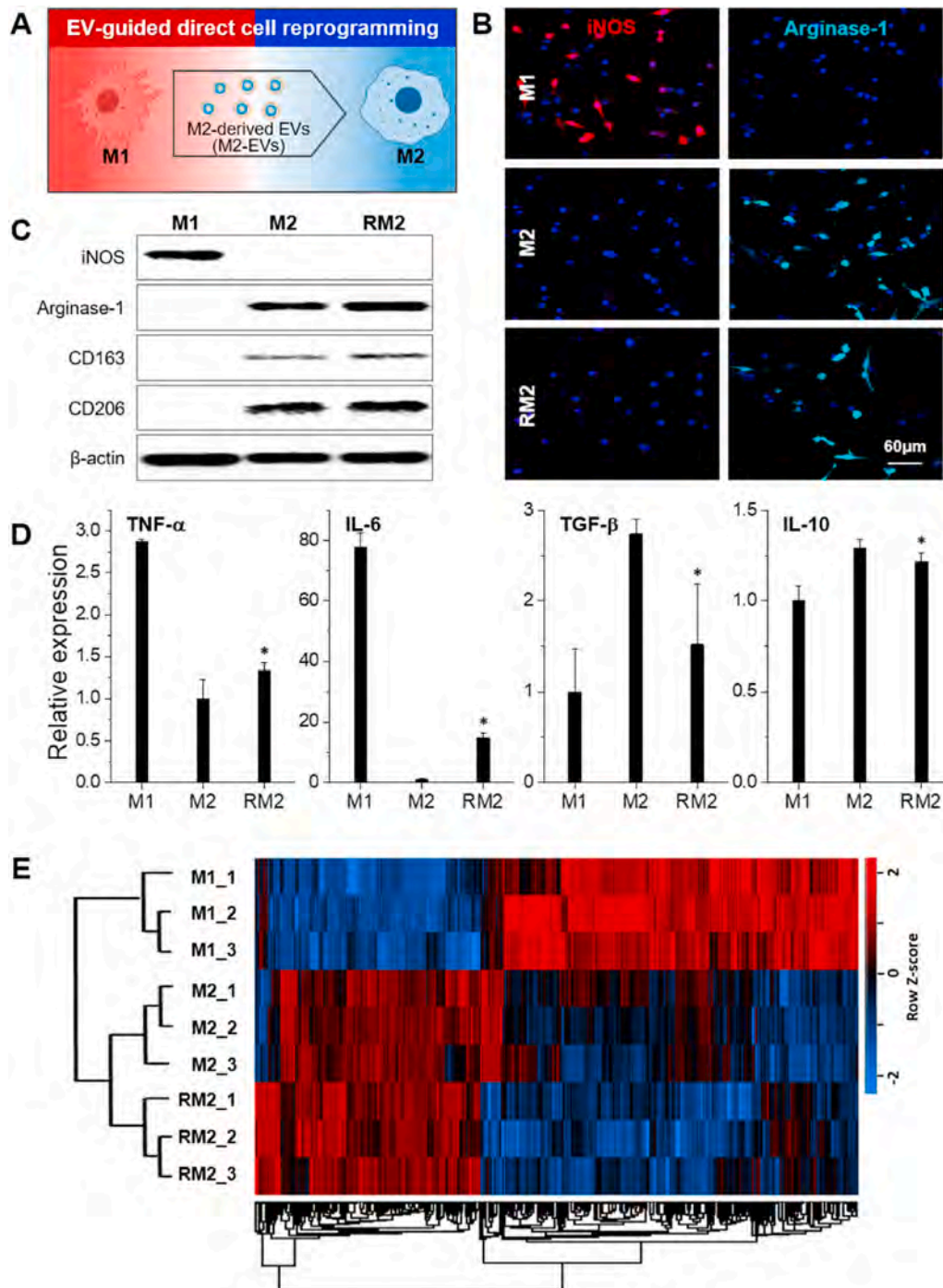


**Fig. 3.** Reprogramming of M1 macrophages into M2 macrophages by M2-EVs. (A) Illustration of M2-EV-guided direct macrophage reprogramming. (B) iNOS and arginase-1 immunostaining in M1, M2 and RM2 macrophages. (C) Western blot analysis of M1, M2 and RM2 macrophages. (D) Relative expression of TNF-α, IL-6, TGF-β and IL-10 genes in M1, M2 and RM2 macrophages by RT-qPCR analysis. Data are presented as means ± SD (n = 6/group; \*p < 0.05 vs. M1 group). (E) Heat map showing hierarchical clustering of 712 proteins with statistically significant changes in abundance (>2.0-fold, p-value < 0.05) in both M2 and RM2 macrophages compared with M1 macrophages. Rows represent each protein and columns are three technical replicates of M1, M2 and RM2 macrophages. Hierarchical clustering of the 712 proteins was performed using Perseus software (1.6.14.0) on log-transformed normalized abundance values after z-score normalization of the data. Hierarchical clustering demonstrated that M2 and RM2 macrophage proteins were clustered together, whereas M1 macrophage proteins clustered independently.

that in M1 macrophages. These results suggest that M2-EVs are highly effective in inducing RM2 macrophages (>90% conversion; Fig. 3B and S1C) that display functional traits of an anti-inflammatory state.

To assess the degree of identity between M2 and RM2 macrophages and differences between M1 and RM2 macrophages at the proteome level, we performed LC-MS/MS analyses on the three types of macrophages. A total of 2490, 2208 and 2154 proteins were identified by LC-MS/MS (performed in triplicate) in M1, M2 and RM2 macrophages, respectively, and 1845 proteins were shared among the three types of macrophages (Fig. S2, Table S1). Label-free quantitative analyses of 2684 proteins in the three types of macrophages based on peak areas revealed significant changes in 1313 proteins ( $p$ -value < 0.05; Table S2). Of these 1313 proteins, 888 proteins showed significant changes between M1 and M2 (>2.0-fold,  $p$ -value < 0.05), and 990 proteins exhibited significant changes between M2 and RM2 (>2.0-fold,  $p$ -value

< 0.05), of which 712 proteins were shared (Fig. S3). Hierarchical clustering analyses of the 712 proteins that exhibited significant changes in common in both M2 and RM2 compared with M1 macrophages showed that proteins in M2 and RM2 groups were clustered together, whereas those of M1 were clustered independently, indicating that RM2 macrophages generated by M2-EV-guided reprogramming exhibit a more M2-like phenotype with the consistent presence of M2-specific proteins (Fig. 3E). In fact, 680 proteins, corresponding to approximately 95% of the 712 proteins in common, exhibited the same increasing or decreasing trends in abundance levels in both M2 and RM2 compared with M1. In particular, arginase-1 (UniprotKB accession: Q61176) showed >52.0-fold and >30.0-fold increases in M2 and RM2 macrophages, respectively, compared with M1 macrophages, and CD206 (Q61830) showed >2.0-fold and >6.0-fold increases in M2 and RM2 macrophages, respectively, compared with M1 macrophages. On

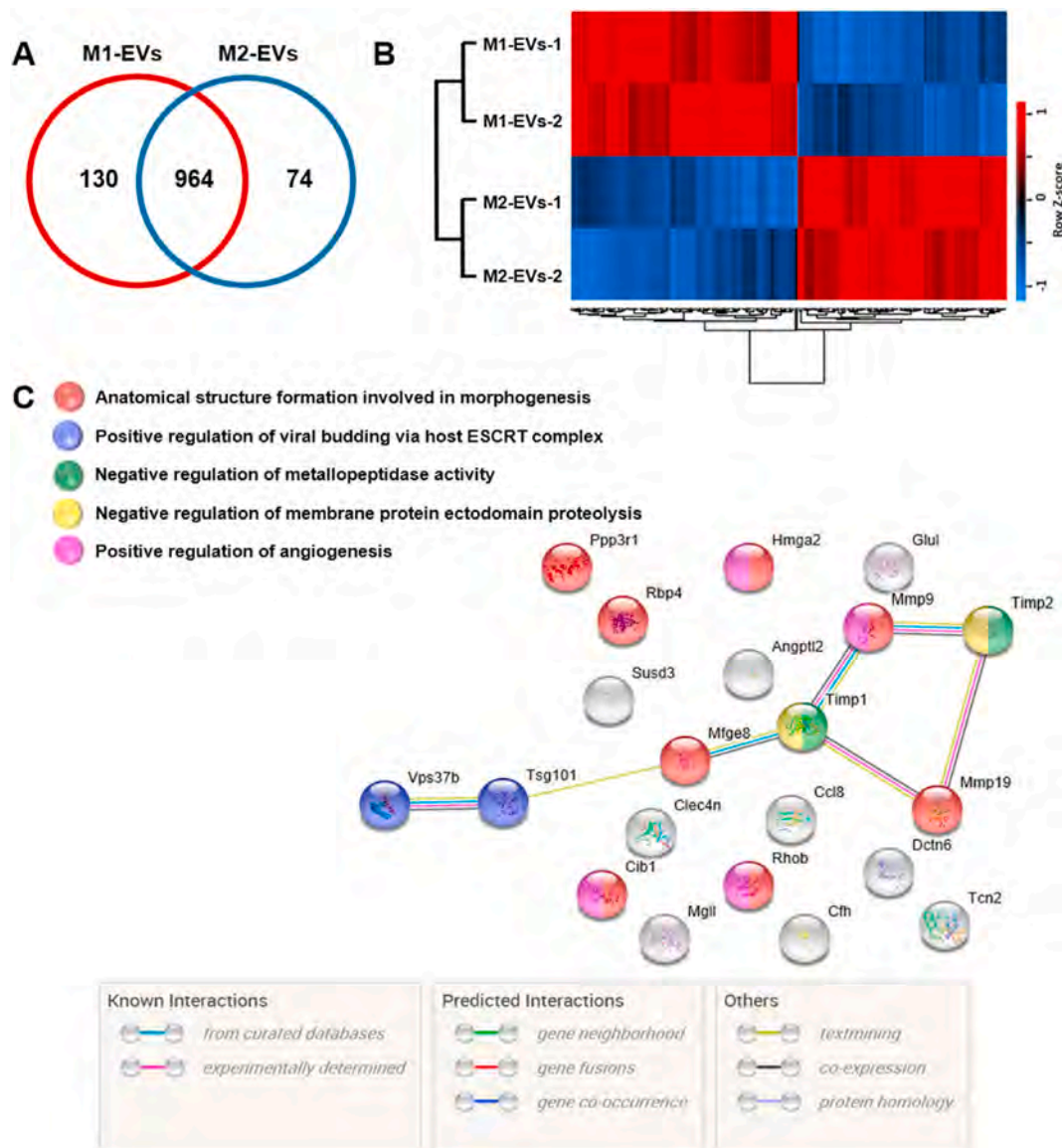


**Fig. 4.** Proteomic analyses of EVs. (A) Venn diagram showing the number of proteins identified by LC-MS/MS analysis in M1-EVs and M2-EVs. Of a total of 1168 proteins identified in the two types of EVs, 1094 were found in M1-EVs and 1038 were identified in M2-EVs. (B) Heat map with dendrogram of hierarchical clustering for two technical replicate LC-MS/MS runs of M1-EVs and M2-EVs. Hierarchical clustering of the 199 proteins was performed using Perseus software on log-transformed normalized abundance values after z-score normalization of the data. (C) STRING interaction enrichment analysis of 20 proteins that were specifically identified in M2-EVs among the identified proteins in M1-EVs and M2-EVs, and M1, M2 and RM2 macrophages. These 20 proteins were significantly increased in M2-EVs compared with M1-EVs based on label-free quantitative analyses. The nodes represent proteins, with color depicting the corresponding biological processes. Colored nodes represent query proteins, and edges display protein-protein interactions. (For interpretation of the references to color in this figure legend, the reader is referred to the Web version of this article.)

the other hand, iNOS (P29477) was decreased >66.0-fold and >312.0-fold in M2 and RM2 macrophages, respectively, compared with M1 macrophages. Thus, proteins that are well known to be specifically up-regulated in M2 (arginase-1, CD206) or M1 (iNOS) macrophages exhibited the same directional changes in abundance in RM2 and M2 macrophages. Next, to further understand the functional implications of up- and down-regulated proteins in M2 and RM2 compared with M1 macrophages, we performed GO enrichment analyses. These analyses showed that, among 346 and 374 proteins that showed significant increases (>2.0-fold,  $p$ -value < 0.05) in M2 and RM2 macrophages, respectively, compared with M1 macrophages identified seven GO biological process (BP) terms—oxidation-reduction process, transport, mitochondrial electron transport, tricarboxylic acid cycle, lipid metabolic process, fatty acid metabolic process and metabolic process—in common among the top 10 GO BP terms that were significantly over-represented in M2 and RM2 macrophages (Fig. S4). As for proteins showing significant decreases in M2 and RM2 compared with M1 macrophages, eight of the top 10 enriched GO BP terms, including immune system process, defense response to virus and response to virus, were shared, implying that RM2 macrophages shared similar biological functions with M2 macrophages. Taken together, these results show that M2-EVs can successfully induce RM2 macrophages with molecular and functional features that closely resemble those of M2 macrophages.

### 3.3. Proteomic analyses of EVs derived from M1 and M2 macrophages

To explore the unique characteristics of M2-EVs, we also performed proteomic analyses of EVs derived from M1 and M2 macrophages and compared their proteomic signatures. LC-MS/MS analyses identified a total of 1094 and 1038 proteins in M1-EVs and M2-EVs, respectively, 964 of which were commonly identified in both samples (Fig. 4A, Table S3). An analysis of 1168 proteins identified in M1-EVs and M2-EVs using DAVID software showed that the most highly enriched cellular component (CC) in both types of EV samples was extracellular vesicle, with 657 proteins being annotated for this CC category (Fig. S5). In addition, TSG10 (Q61187), CD81 antigen (CD81; P35762), programmed cell death 6-interacting protein (Alix; Q9WU78) and CD9 antigen (CD9; P40240), which are known as EV-specific markers, have been confidently identified in EV samples [42,43]. Label-free quantitative analyses of 1166 proteins based on peak areas between the two types of EV samples showed significant changes in 226 proteins ( $p$ -value < 0.05; Table S4). Of these proteins, 98 proteins exhibited >2.0-fold increases in M2-EVs, whereas 101 proteins showed >2.0-fold increases in M1-EVs. Arginase-1 and CD206, known to be up-regulated in M2 macrophages [44,45], showed >37.0-fold and >143.0-fold increases, respectively, in M2-EV samples, indicating that M2-EVs possess similar characteristics specific to M2 macrophages. On the other hand, iNOS was significantly increased (>189.0-fold) in M1-EV samples. A hierarchical clustering analysis of 199 proteins that exhibited statistically significant changes ( $p$ -value < 0.05, >2.0-fold) between M1-EV and M2-EV samples showed clearly distinct protein expression patterns between the two types of EVs (Fig. 4B).

We next attempted to determine which components of M2-EVs played major roles in the reprogramming process that converts M1 into M2 macrophages. First, a Venn diagram analysis was performed using lists of identified proteins from M1-EVs and M2-EVs, and M1, M2 and RM2 macrophages with more than two unique peptides (Fig. S6). This analysis specifically identified 29 proteins in M2-EVs. We then explored whether these 29 proteins were detected in other types of EV samples in addition to M2-EVs. We found that, of the 29 proteins, 28 proteins were also detected in the M1-EV sample; the remaining protein, transcobalamin-2 (O88968), known as primary vitamin B12-binding and transport protein, was only detected in M2-EVs [46]. None of the 29 proteins were detected in M1, M2 and RM2 macrophages. Of the 29 proteins, 20 proteins were significantly increased (>2.0-fold,  $p$ -value < 0.05) in M2-EVs compared with M1-EVs (Table S5). We next examined

the functional interaction networks of the 20 proteins specific to M2-EVs using a STRING interaction enrichment analysis (Fig. 4C). In addition to providing a visualization of the functional association networks of the proteins, this STRING analysis revealed enrichment of the top five GO BP terms, including positive regulation of viral budding via host ESCRT complex, angiogenesis related to EV biogenesis and M2 macrophage-like property [47,48]. Among those proteins showing significant up-regulation in M2-EVs, MMP19 (Q9JH10) and CCL8 (Q9Z121) possess anti-inflammatory properties and are known to regulate the generation and migration of M2 macrophages into inflamed tissues as part of the resolution phase [49,50]. In addition, glutamine synthetase (P15105) has been reported to play a pivotal role in the metabolic network for M2 macrophage polarization, and MFG-E8 (P21956) was previously found to promote the transformation of macrophages to M2 subtype [21,51,52]. Collectively, these findings suggest that these proteins in M2-EVs act through complex interactions to induce the reprogramming of M1 into M2 macrophages.

### 3.4. *In vivo* therapeutic effects of M2-EV-guided macrophage reprogramming in collagen-induced arthritis mice

Prior to examining the therapeutic effects of M2-EVs in a collagen-induced arthritis (CIA) mouse model, we investigated the bio-distribution of EVs in these mice to determine the optimal administration route and schedule (Fig. 5). Cyanine 5.5-labeled M2-EVs administered via footpad injection were maintained at a very high concentration in the ankle joints of the hind limb for about 4 days and were detectable for up to 12 days (Fig. 5A). The fluorescence of free cyanine-5.5 was significantly reduced only 1 day after injection and did not affect the biodistribution of EVs (Data not shown). Intra-articular (IA) administration of M2-EVs yielded a biodistribution similar to that of footpad injection (Fig. S7); in contrast, M2-EVs administered via intravenous (IV) or subcutaneous (SC) routes tended to be eliminated from the body within 2–3 days. Thus, local administration leads to enhanced accumulation and prolonged sequestration of EVs in articular tissues, likely due to a combination of slow distribution dynamics via microvascular or lymphatic pathways and enhanced capillary permeability by joint inflammation [53,54]. Unlike small molecules, which show rapid efflux from the joint following intra-articular injection [55,56], EVs, with their extended intra-articular retention times, can provide sustained action for RA therapy after local injection. The particle size of M2-EVs (~100 nm) is advantageous in this regard, enabling their rapid entry into articular tissue compartments and subsequent extended retention via an endothelial permeability and retention (EPR)-like effect reminiscent of that which has been extensively explored for passive tumor targeting of nanoparticles [57], thereby providing less of an opportunity for EVs to permeate into other normal tissues. Consistent with this, an assessment of the tissue distribution of M2-EVs 4 days after footpad injection showed that M2-EVs tended to be less widely distributed, primarily to the liver and kidneys (Fig. 5B and C). However, a large fraction of M2-EVs were still retained in the hind paw, predicting prolonged duration of EV action.

On the basis of these results, we chose to administer 100  $\mu$ g of M2-EVs in a volume of 20  $\mu$ L every 4 days via s.c. footpad injection into CIA model mice as an *in vivo* RA treatment paradigm. Among traditional DMARDs, which are typically synthetic small molecule drugs with anti-inflammatory function, Methotrexate (MTX), the first-line drug for the clinical treatment of RA, was used here as a positive control [58]. The *in vivo* therapeutic efficacy of EV treatments was monitored over a 50-day period after the first immunization of CIA mice (Fig. 6A–C). The severity of joint inflammation and swelling was used as a direct indicator of RA, and clinical scores (scale, 0 to 4) were assigned to forelimbs and hind limbs [27]. Fully developed arthritis, including swollen paw and erythema, was observed from day 21 after the first immunization. Administration of MTX or M2-EVs slowed RA progression, significantly reducing average arthritis scores to 4.1 and 6.2, respectively, with

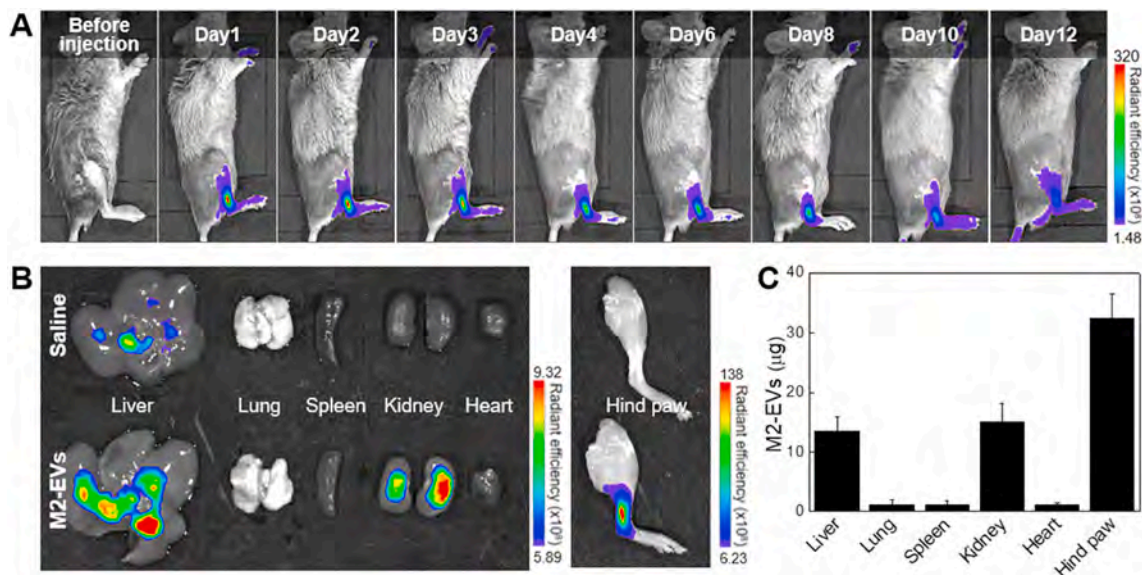


**Fig. 5.** *In vivo* biodistribution of EVs. (A) Real-time *in vivo* imaging after footpad injection of Cy5.5-NHS labeled M2-EVs. (B) *Ex vivo* imaging of hind paws and major organs at day 4 after mice were treated with M2-EVs. (C) Quantitative tissue distribution data for M2-EVs on day 4 after footpad injection of M2-EVs. Data are presented means  $\pm$  SD ( $n = 6$ /group).

corresponding mean paw thicknesses of 7.9 and 8.7. By comparison, mice in the saline-treated group exhibited a severe course of RA with no resolution phase and reached a significantly higher arthritic score (average, 12.2) compared with mice in MTX- and M2-EV-treated groups. In addition, paw temperature, measured as an additional feature of inflammation in CIA mice using an infrared thermal scanning camera (Fig. 6D), was higher in saline-treated arthritis mice ( $34.1 \pm 0.5$  °C) than in untreated control mice ( $28.3 \pm 0.2$  °C;  $p < 0.01$ ), and was significantly attenuated in mice treated with MTX ( $30.2 \pm 0.7$  °C,  $p < 0.05$ ) or M2-EVs ( $30.4 \pm 0.5$  °C,  $p < 0.01$ ) compared with saline-treated arthritis model mice. The improvements in clinical indices observed with administration of M2-EVs were accompanied by significantly suppressed production of joint-associated inflammatory cytokines compared with saline injection (Fig. 6E). In particular, the protein expression levels of TNF- $\alpha$  and IL-6 decreased 1.7- and 3.5-fold, respectively, in the M2-EV group compared with the saline group. These results confirm the effectiveness of M2-EV-guided reprogramming in suppressing inflammatory responses and RA progression, demonstrating that the efficacy of M2-EV treatment is comparable to that of the conventional RA drug, MTX. Considering that traditional DMARDs cause a spectrum of toxic side effects, including gastrointestinal damage [59,60], the EV-based approach may offer advantages over MTX. Indeed, TUNEL assays showed a remarkable increase in the number of apoptotic cells in small intestinal crypts and villi in MTX-treated mice (Fig. 6F, green), whereas no apoptotic cell death was observed in the intestinal mucosa of M2-EV-treated mice. Even after the administration of both MTX and M2-EVs via footpad injection, the AST and ALT levels, which are indicators of liver toxicity, were increased significantly only in the MTX-treated group, whereas there was no detectable change in the M2-EV-treated group compared to the saline group (Fig. S10). As a result, it shows that the superiority of M2-EVs in toxicity over MTX is due to the difference in the type of drugs themselves, not the difference in the route of administration.

For histological examinations of synovial tissues, paws were harvested 45 days after the first immunization and stained with hematoxylin and eosin (H&E) and Safranin O (Fig. 7A and B). Notably, the histopathological status of MTX and M2-EV-treated mice was similar to that of normal healthy mice. Thus, treatment with MTX or M2-EVs significantly attenuated cartilage erosion, neutrophil infiltration and synovial hyperplasia (Fig. 7C–E). To further assess the impact of M2-EV

treatment on bone destruction in CIA mice, we monitored the bone tissues of hind paws using *ex vivo* high-resolution micro-CT imaging. Severe joint bone erosion was observed in saline-treated mice (Fig. 7F), whereas mice in the M2-EV-treated group displayed an intact joint structure with a smooth bone surface, indicating that M2-EVs successfully prevented inflammatory bone destruction in the CIA mouse model.

### 3.5. EV-guided *in situ* reprogramming of M1 into M2 macrophages in joints of collagen-induced arthritis mice

To explore the reprogramming of pro-inflammatory M1 macrophages into anti-inflammatory M2 macrophages *in vivo*, we first assessed the expression of specific phenotypic markers of M1 (iNOS) and M2 (CD206) macrophages in arthritic joint sections from CIA mice by immunohistochemical analysis (Fig. 8A and B). iNOS expression was markedly increased in the joint tissues of saline-treated CIA mice. M2-EV treatment simultaneously decreased iNOS expression and increased CD206 expression, implying an efficient switch of synovial macrophages toward M2 phenotype. In contrast, CIA model mice treated with MTX exhibited drastic decreases in both iNOS and CD 206 expression, indicating significant depletion of synovium-resident macrophages. Decreases in synovium-resident macrophages can precede the symptoms of RA, reflecting the fact that such a macrophage-depleted environment is detrimental to the healing process of damaged muscles, bones, tendons and ligaments [1,61]. In fact, the representative mechanism of action of MTX in RA treatment is its well-known promotion of adenosine release and subsequent adenosine-mediated inhibition of inflammation through binding to specific receptors on the surface of lymphocytes, monocytes and neutrophils [62]. However, by interfering with the trans-methylation reaction, which is important for functional activation of various biological compounds, including proteins and lipids, MTX treatment concurrently suppresses the function of these immune effector cells [63]. Thus, there are still remaining concerns about potential long-term consequences of MTX treatment, despite its well-known benefits.

Phenotypic changes in the synovial macrophage subpopulation were further explored using flow cytometry analysis (Fig. 8B). The results of this analysis were consistent with the results of immunohistochemical analyses. After the administration of M2-EVs, disease-associated increases in the M1 macrophage (F4/80+) population in CIA mice were

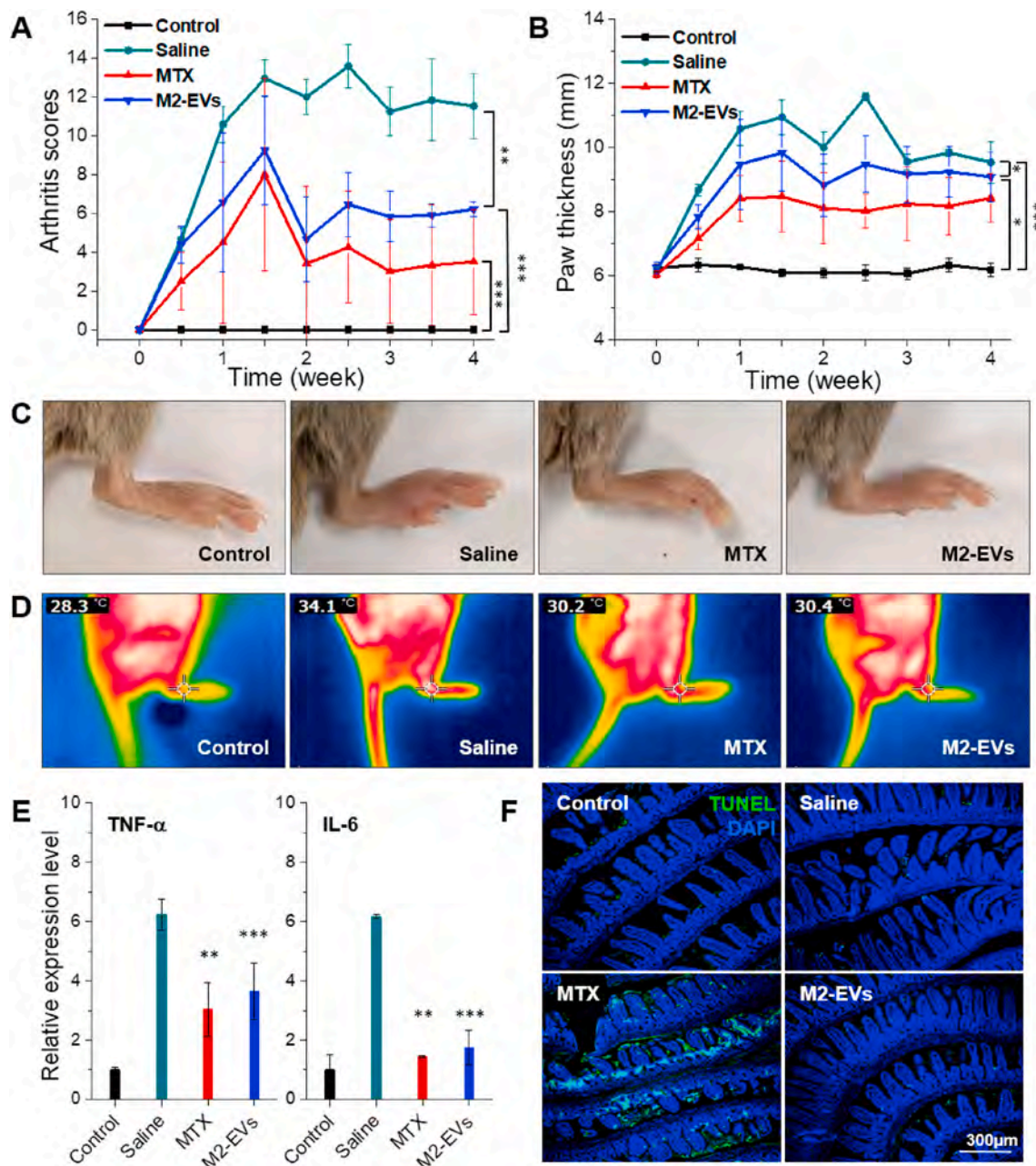


**Fig. 6.** *In vivo* therapeutic efficacy of M2-EVs in CIA model mice. (A) Mean clinical score measurements and (B) paw thickness of CIA mice treated with saline, MTX, or M2-EVs. PBS and M2-EVs (100 µg/20 µL) were injected into footpads of mice, and MTX (2.5 mg/kg) was injected intraperitoneally every 4 days. (C, D) Representative images of hind paws in different treatment groups obtained with a conventional (C) or infrared (D) camera. (E) Relative expression of TNF-α and IL-6 genes in joint tissue of different treatment groups. All data are presented as means ± SD (n = 6/group; \*\*\*p < 0.001, \*\*p < 0.001 and \*p < 0.05 vs. control). (F) Representative images of TUNEL (terminal deoxynucleotidyl transferase dUTP nick-end labeling)-stained sections of small intestine tissues from normal and CIA model mice treated with saline, MTX, or M2-EVs.

decreased from 13.4% ± 4.2%–9.6% ± 2.8% in association with an increase in the M2 macrophage (CD206+) population from 6.2% ± 2.2%–8.1% ± 3.0%. As expected, the overall population of synovial macrophages in MTX-treated mice also decreased compared with that in normal healthy mice.

Finally, to directly confirm M2-EV-guided macrophage reprogramming in the synovial joint, we injected fluorescence-labeled M1 macrophages intra-articularly together with M2-EVs and performed a flow cytometry analysis 1 day later (Fig. 8C). This analysis showed that ~24% of fluorescently pre-labeled M1 macrophages were switched to M2 macrophages (CD206+), strongly supporting the conclusion that M2-EVs enable *in situ* reprogramming of resident macrophages toward

M2 phenotype.

#### 4. Conclusion

Collectively, our results demonstrate that M2-EVs, which show rapid accumulation and extended retention within articular tissue, can successfully re-establish the M1-M2 macrophage equilibrium in RA synovial tissue by very effectively switching pro-inflammatory M1 to anti-inflammatory M2 macrophages. Thus, M2-EV-guided *in situ* macrophage reprogramming toward anti-inflammatory M2 macrophages clearly ameliorates synovial inflammation and protects against joint destruction in CIA mice, producing anti-arthritic activity comparable to

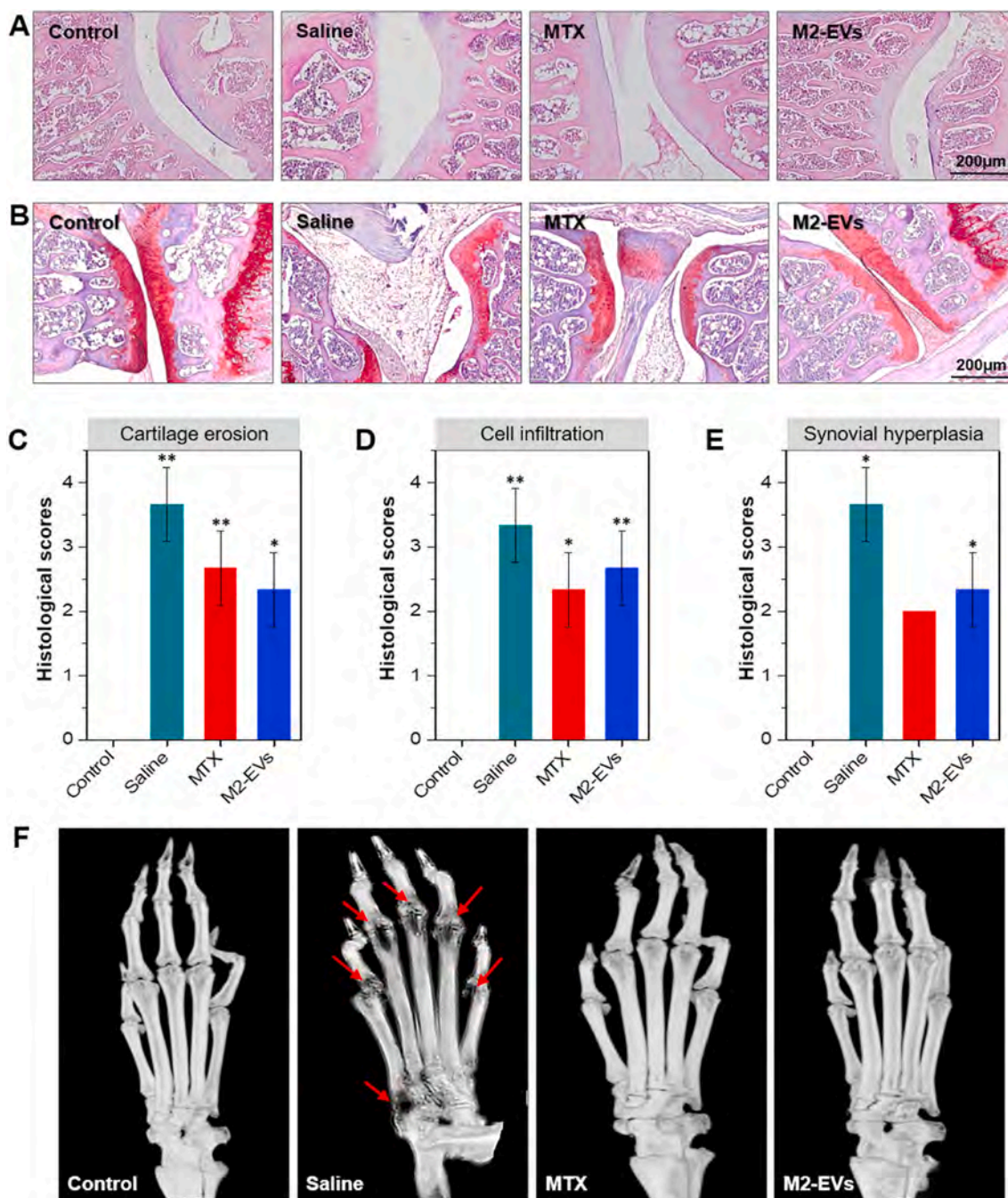


**Fig. 7.** Histological assessment of arthritic joints in CIA model mice. (A) H&E staining and (B) Safranin O staining of ankle joints excised from mice. (C–E) Histological scores of cartilage erosion (C), cell infiltration (D) and synovial hyperplasia (E). All data are presented as means  $\pm$  SD ( $n = 6$ /group; \*\* $p < 0.001$  and \* $p < 0.05$  vs. control). (F) Representative 3D-reconstructed images of hind paws by microCT analysis showing bone degradation (red arrows). (For interpretation of the references to color in this figure legend, the reader is referred to the Web version of this article.)

that of MTX, but without the several potential adverse effects associated with this latter traditional DMARD. In addition to serving as a promising source of acellular therapy, EVs as drug-delivery vehicles can be further exploited for the manufacture of targeting ligands and biological therapeutics through additional engineering. However, there are still several barriers to overcome before clinical use of EVs, such as low productivity of EVs, heterogeneity, and analysis of key components that cause therapeutic or adverse effects. Therefore, along with in-depth studies to overcome these barriers, M2-EV-guided reprogramming for *in situ* tuning of macrophage responses can be utilized as a highly effective and safe anti-inflammatory therapeutic strategy for various inflammation-related diseases, including RA.

#### Data availability

The raw data required to reproduce these findings are available from the authors upon request.

#### CRediT authorship contribution statement

**Hyosuk Kim:** Conceptualization, Methodology, Validation, Investigation, Data curation, Writing – original draft. **Ji Hyun Back:** Methodology, Validation, Investigation, Writing – original draft. **Geonhee Han:** Validation, Investigation. **Su Jin Lee:** Validation, Investigation. **Yae Eun Park:** Validation, Investigation. **Man Bock Gu:** Visualization.

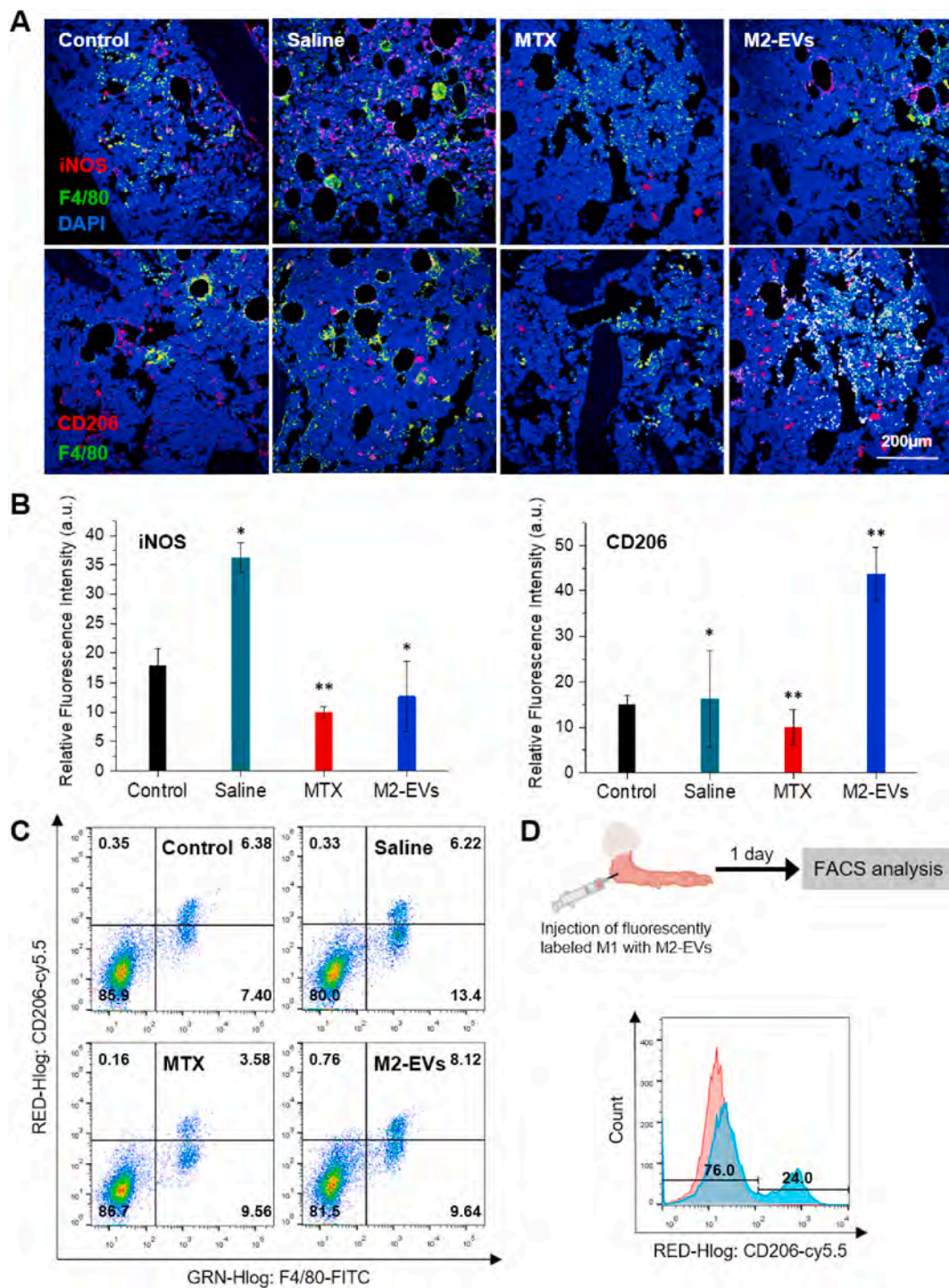


**Fig. 8.** *In situ* macrophage reprogramming in arthritic joints of CIA model mice by M2-EVs. (A) Representative images of arthritic joint sections stained with macrophage-specific marker F4/80 and M1 and M2 macrophage markers iNOS and CD206, respectively. (B) Quantification analysis of the expression of iNOS and CD206 in mouse joint tissue. All data are presented as means  $\pm$  SD ( $n = 3/\text{group}$ ; \*\* $p < 0.001$  and \* $p < 0.05$  vs. control). (C) Flow cytometry analysis of M1 and M2 macrophage populations in synovial tissue in different treatment groups. (D) Flow cytometry analysis of *in situ* macrophage reprogramming by M2-EVs in synovial tissue. CD206-positive cells from the labeled macrophage population were analyzed by flow cytometry 24 h after co-injecting M1 macrophages labeled with Cell-Tracker Green CMFDA and M2-EVs into the joint. (For interpretation of the references to color in this figure legend, the reader is referred to the Web version of this article.)

**Yoosoo Yang:** Visualization. **Ji Eun Lee:** Writing – review & editing, Supervision, Funding acquisition. **Sun Hwa Kim:** Writing – review & editing, Supervision, Funding acquisition.

**Declaration of competing interest**

The authors declare that they have no known competing financial interests or personal relationships that could have appeared to influence the work reported in this paper.

## Acknowledgments

This work was supported by the International Research & Development Program (NRF-2019K1A4A7A02102530) and Brain Pool Program (NRF-2020H1D3A1A02081401) funded by the Ministry of Science and ICT, the Korea Health Technology R&D Project through the Korea Health Industry Development Institute funded by the Ministry of Health and Welfare (HI20C0013), Samsung Research Funding & Incubation Center of Samsung Electronics (SRFC-MA1901-10) and by the KIST Institutional Program.

## Appendix A. Supplementary data

Supplementary data to this article can be found online at <https://doi.org/10.1016/j.biomaterials.2022.121578>.

## References

- [1] R.W. Kinne, B. Stuhlmueller, G.R. Burmester, Cells of the synovium in rheumatoid arthritis. *Macrophages, Arthritis Res. Ther.* 9 (6) (2007) 224.
- [2] S.K. Biswas, A. Mantovani, Macrophage plasticity and interaction with lymphocyte subsets: cancer as a paradigm. *Nat. Immunol.* 11 (10) (2010) 889–896.
- [3] A. Mantovani, S.K. Biswas, M.R. Galdiero, A. Sica, M. Locati, Macrophage plasticity and polarization in tissue repair and remodeling. *J. Pathol.* 229 (2) (2013) 176–185.
- [4] J. Li, H.C. Hsu, J.D. Mountz, Managing macrophages in rheumatoid arthritis by reform or removal. *Curr. Rheumatol. Rep.* 14 (5) (2012) 445–454.
- [5] Y. Wang, C.C. Han, D. Cui, Y. Li, Y. Ma, W. Wei, Is macrophage polarization important in rheumatoid arthritis? *Int. Immunopharm.* 50 (2017) 345–352.
- [6] I. Padjen, M.R. Crnogaj, B. Anic, Conventional disease-modifying agents in rheumatoid arthritis - a review of their current use and role in treatment algorithms. *Reumatologia* 58 (6) (2020) 390–400.
- [7] Y. Bedoui, X. Guillot, J. Selambarom, P. Guiraud, C. Giry, M.C. Jaffar-Bandjee, S. Ralandison, P. Gasque, Methotrexate an old drug with new tricks. *Int. J. Mol. Sci.* 20 (20) (2019).
- [8] T.K. Mwangi, I.M. Berke, E.H. Nieves, R.D. Bell, S.B. Adams, L.A. Setton, Intra-articular clearance of labeled dextrans from naive and arthritic rat knee joints. *J. Contr. Release* 283 (2018) 76–83.
- [9] C. Song, S. Xu, L. Chang, X. Zhao, X. Mei, X. Ren, Z. Chen, Preparation of EGCG decorated, injectable extracellular vesicles for cartilage repair in rat arthritis. *Regen. Biomater.* 8 (6) (2021), rbab067.
- [10] M. Takemaka, A. Yabuta, Y. Takahashi, Y. Takakura, Interleukin-4-carrying small extracellular vesicles with a high potential as anti-inflammatory therapeutics based on modulation of macrophage function. *Biomaterials* 278 (2021) 121160.
- [11] Q. Zhang, D. Dehaini, Y. Zhang, J. Zhou, X. Chen, L. Zhang, R.H. Fang, W. Gao, L. Zhang, Neutrophil membrane-coated nanoparticles inhibit synovial inflammation and alleviate joint damage in inflammatory arthritis. *Nat. Nanotechnol.* 13 (12) (2018) 1182–1190.
- [12] P. Barrera, A. Blom, P.L. van Lent, L. van Bloois, J.H. Beijnen, N. van Rooijen, M. C. de Waal Malefijt, L.B. van de Putte, G. Storm, W.B. van den Berg, Synovial macrophage depletion with clodronate-containing liposomes in rheumatoid arthritis. *Arthritis Rheum.* 43 (9) (2000) 1951–1959.
- [13] P.J. Richards, A.S. Williams, R.M. Goodfellow, B.D. Williams, Liposomal clodronate eliminates synovial macrophages, reduces inflammation and ameliorates joint destruction in antigen-induced arthritis. *Rheumatology* 38 (9) (1999) 818–825.
- [14] J.A. van Roon, J.W. Bijlsma, J.G. van de Winkel, F.P. Lafeber, Depletion of synovial macrophages in rheumatoid arthritis by an anti-FcγRIIb-calicheamicin immunconjugate. *Ann. Rheum. Dis.* 64 (6) (2005) 865–870.
- [15] Q. Zhang, R. Yuan, C. Li, W. Wei, W. Shen, Y. Cui, X. Yuan, Macrophage depletion with clodronate-containing liposomes affects the incidence and development of rheumatoid arthritis. *Z. Rheumatol.* 78 (10) (2019) 996–1003.
- [16] R. Li, Y. He, Y. Zhu, L. Jiang, S. Zhang, J. Qin, Q. Wu, W. Dai, S. Shen, Z. Pang, J. Wang, Route to rheumatoid arthritis by macrophage-derived microvesicle-coated nanoparticles. *Nano Lett.* 19 (1) (2019) 124–134.
- [17] Y. Yang, L. Guo, Z. Wang, P. Liu, X. Liu, J. Ding, W. Zhou, Targeted silver nanoparticles for rheumatoid arthritis therapy via macrophage apoptosis and Repolarization. *Biomaterials* 264 (2021) 120390.
- [18] J. Phan, P. Kumar, D. Hao, K. Gao, D. Farmer, A. Wang, Engineering mesenchymal stem cells to improve their exosome efficacy and yield for cell-free therapy. *J. Extracell. Vesicles* 7 (1) (2018) 1522236.
- [19] Z.J. Smith, C. Lee, T. Rojalin, R.P. Carney, S. Hazari, A. Knudson, K. Lam, H. Saari, E.L. Ibanez, T. Viitala, T. Laaksonen, M. Yliperttula, S. Wachsmann-Hogiu, Single exosome study reveals subpopulations distributed among cell lines with variability related to membrane content. *J. Extracell. Vesicles* 4 (2015) 28533.
- [20] H. Valadi, K. Ekstrom, A. Bossios, M. Sjostrand, J.J. Lee, J.O. Lotvall, Exosome-mediated transfer of mRNAs and microRNAs is a novel mechanism of genetic exchange between cells. *Nat. Cell Biol.* 9 (6) (2007) 654–659.
- [21] H. Kim, S.Y. Wang, G. Kwak, Y. Yang, I.C. Kwon, S.H. Kim, Exosome-guided phenotypic switch of M1 to M2 macrophages for cutaneous wound healing. *Adv. Sci.* 6 (20) (2019) 1900513.
- [22] C. Thery, S. Amigorena, G. Raposo, A. Clayton, Isolation and characterization of exosomes from cell culture supernatants and biological fluids. *Curr. Protoc. Cell Biol. Chapter 3* (2006). Unit 3 22.
- [23] P. Li, M. Kaslan, S.H. Lee, J. Yao, Z. Gao, Progress in Exosome Isolation Techniques. *Theranostics* 7 (3) (2017) 789–804.
- [24] S. Tyanova, T. Temu, P. Sinitcyn, A. Carlson, M.Y. Hein, T. Geiger, M. Mann, J. Cox, The Perseus computational platform for comprehensive analysis of (prote) omics data. *Nat. Methods* 13 (9) (2016) 731–740.
- [25] D. Szklarczyk, J.H. Morris, H. Cook, M. Kuhn, S. Wyder, M. Simonovic, A. Santos, N.T. Doncheva, A. Roth, P. Bork, L.J. Jensen, C. von Mering, The STRING database in 2017: quality-controlled protein-protein association networks, made broadly accessible. *Nucleic Acids Res.* 45 (D1) (2017) D362–D368.
- [26] J.J. Inglis, E. Simelyte, F.E. McCann, G. Criado, R.O. Williams, Protocol for the induction of arthritis in C57BL/6 mice. *Nat. Protoc.* 3 (4) (2008) 612–618.
- [27] D.D. Brand, K.A. Latham, E.F. Rosloniec, Collagen-induced arthritis. *Nat. Protoc.* 2 (5) (2007) 1269–1275.
- [28] J.D. Bailey, A. Shaw, E. McNeill, T. Nicol, M. Diotallevi, S. Chuaiphichai, J. Patel, A. Hale, K.M. Channon, M.J. Crabtree, Isolation and culture of murine bone marrow-derived macrophages for nitric oxide and redox biology. *Nitric Oxide* 100–101 (2020) 17–29.
- [29] M. Depke, K. Breitbach, K. Dinh Hoang Dang, L. Brinkmann, M.G. Salazar, V. M. Dhople, A. Bast, L. Steil, F. Schmidt, I. Steinmetz, U. Volker, Bone marrow-derived macrophages from BALB/c and C57BL/6 mice fundamentally differ in their respiratory chain complex proteins, lysosomal enzymology and components of antioxidant stress systems. *J. Proteomics* 103 (2014) 72–86.
- [30] B.S. Joshi, M.A. de Beer, B.N.G. Giepmans, I.S. Zuhorn, Endocytosis of extracellular vesicles and release of their cargo from endosomes. *ACS Nano* 14 (4) (2020) 4444–4455.
- [31] L. Czernek, A. Chworos, M. Duechler, The uptake of extracellular vesicles is affected by the differentiation status of myeloid cells. *Scand. J. Immunol.* 82 (6) (2015) 506–514.
- [32] K.C. French, M.A. Antonyak, R.A. Cerione, Extracellular vesicle docking at the cellular port: extracellular vesicle binding and uptake. *Semin. Cell Dev. Biol.* 67 (2017) 48–55.
- [33] S.N. Hurwitz, M.A. Rider, J.L. Bundy, X. Liu, R.K. Singh, D.G. Meckes Jr., Proteomic profiling of NCI-60 extracellular vesicles uncovers common protein cargo and cancer type-specific biomarkers. *Oncotarget* 7 (52) (2016) 86999–87015.
- [34] G. Marostica, S. Gelibter, M. Gironi, A. Nigro, R. Furlan, Extracellular vesicles in neuroinflammation. *Front. Cell Dev. Biol.* 8 (2020) 623039.
- [35] S. Tardito, G. Martinelli, S. Soldano, S. Paolino, G. Pacini, M. Patane, E. Alessandri, V. Smith, M. Cutolo, Macrophage M1/M2 polarization and rheumatoid arthritis: a systematic review. *Autoimmun. Rev.* 18 (11) (2019) 102397.
- [36] I.A. Udalova, A. Mantovani, M. Feldmann, Macrophage heterogeneity in the context of rheumatoid arthritis. *Nat. Rev. Rheumatol.* 12 (8) (2016) 472–485.
- [37] B. Kim, J.H. Lee, W.J. Jin, H.H. Kim, H. Ha, Z.H. Lee, JN-2, a C-X-C motif chemokine receptor 3 antagonist, ameliorates arthritis progression in an animal model. *Eur. J. Pharmacol.* 823 (2018) 1–10.
- [38] T. Matsumoto, N. Takahashi, T. Kojima, Y. Yoshioka, J. Ishikawa, K. Furukawa, K. Ono, M. Sawada, N. Ishiguro, A. Yamamoto, Soluble Siglec-9 suppresses arthritis in a collagen-induced arthritis mouse model and inhibits M1 activation of RAW264.7 macrophages. *Arthritis Res. Ther.* 18 (1) (2016) 133.
- [39] E.L. Mills, B. Kelly, A. Logan, A.S.H. Costa, M. Varma, C.E. Bryant, P. Tourlamos, J.H.M. Dabritz, E. Gottlieb, I. Latorre, S.C. Corr, G. McManus, D. Ryan, H.T. Jacobs, M. Szibor, R.J. Xavier, T. Braun, C. Frezza, M.P. Murphy, L.A. O'Neill, Succinate dehydrogenase supports metabolic repurposing of mitochondria to drive inflammatory macrophages. *Cell* 167 (2) (2016), 457–470 e13.
- [40] M. Siebelt, N. Korthagen, W. Wei, H. Groen, Y. Bastiaansen-Jenniskens, C. Muller, J.H. Waarsing, M. de Jong, H. Weinans, Triamcinolone acetonide activates an anti-inflammatory and folate receptor-positive macrophage that prevents osteophytosis in vivo. *Arthritis Res. Ther.* 17 (2015) 352.
- [41] M. Zhu, B. Yu, J. Bai, X. Wang, X. Guo, Y. Liu, J. Lin, S. Hu, W. Zhang, Y. Tao, C. Hu, H. Yang, Y. Xu, D. Geng, Cannabinoid receptor 2 agonist prevents local and systemic inflammatory bone destruction in rheumatoid arthritis. *J. Bone Miner. Res.* 34 (4) (2019) 739–751.
- [42] P. Zheng, Q. Luo, W. Wang, J. Li, T. Wang, P. Wang, L. Chen, P. Zhang, H. Chen, Y. Liu, P. Dong, G. Xie, Y. Ma, L. Jiang, X. Yuan, L. Shen, Tumor-associated macrophages-derived exosomes promote the migration of gastric cancer cells by transfer of functional Apolipoprotein E. *Cell Death Dis.* 9 (4) (2018) 434.
- [43] J. Zhu, B. Liu, Z. Wang, D. Wang, H. Ni, L. Zhang, Y. Wang, Exosomes from nicotine-stimulated macrophages accelerate atherosclerosis through miR-21-3p/PEN-mediated VSMC migration and proliferation. *Theranostics* 9 (23) (2019) 6901–6919.
- [44] T. Kreider, R.M. Anthony, J.F. Urban Jr., W.C. Gause, Alternatively activated macrophages in helminth infections. *Curr. Opin. Immunol.* 19 (4) (2007) 448–453.
- [45] Y.C. Liu, X.B. Zou, Y.F. Chai, Y.M. Yao, Macrophage polarization in inflammatory diseases. *Int. J. Biol. Sci.* 10 (5) (2014) 520–529.
- [46] B. Rachmilewitz, M. Rachmilewitz, M. Chaouat, M. Schlesinger, The synthesis of transcobalamin II, a vitamin B12 transport protein, by stimulated mouse peritoneal macrophages. *Biomedicine* 27 (6) (1977) 213–214.
- [47] M. Colombo, C. Moita, G. van Niel, J. Kowal, J. Vigneron, P. Benaroch, N. Manel, L. F. Moita, C. Thery, G. Raposo, Analysis of ESCRT functions in exosome biogenesis, composition and secretion highlights the heterogeneity of extracellular vesicles. *J. Cell Sci.* 126 (Pt 24) (2013) 5553–5565.
- [48] S. Quintero-Fabian, R. Arreola, E. Becerril-Villanueva, J.C. Torres-Romero, V. Arana-Argaez, J. Lara-Riegos, M.A. Ramirez-Camacho, M.E. Alvarez-Sanchez,

- Role of matrix metalloproteinases in angiogenesis and cancer, *Front. Oncol.* 9 (2019) 1370.
- [49] E. Farmaki, V. Kaza, I. Chatzistamou, H. Kiaris, CCL8 promotes postpartum breast cancer by recruiting M2 macrophages, *iScience* 23 (6) (2020) 101217.
- [50] B. Fingleton, Matrix metalloproteinases as regulators of inflammatory processes, *Biochim. Biophys. Acta Mol. Cell Res.* 1864 (11 Pt A) (2017) 2036–2042.
- [51] A.K. Jha, S.C. Huang, A. Sergushichev, V. Lampropoulou, Y. Ivanova, E. Loginicheva, K. Chmielewski, K.M. Stewart, J. Ashall, B. Everts, E.J. Pearce, E. M. Driggers, M.N. Artyomov, Network integration of parallel metabolic and transcriptional data reveals metabolic modules that regulate macrophage polarization, *Immunity* 42 (3) (2015) 419–430.
- [52] P. Laplante, F. Brillant-Marquis, M.J. Brissette, B. Joannette-Pilon, R. Cayrol, V. Kokta, J.F. Cailhier, MFG-E8 reprogramming of macrophages promotes wound healing by increased bFGF production and fibroblast functions, *J. Invest. Dermatol.* 137 (9) (2017) 2005–2013.
- [53] D.M. McDonald, Endothelial gaps: plasma leakage during inflammation, *News Physiol. Sci.* 13 (1998) 104–105.
- [54] J. Pradal, P. Maudens, C. Gabay, C.A. Seemayer, O. Jordan, E. Allemann, Effect of particle size on the biodistribution of nano- and microparticles following intra-articular injection in mice, *Int. J. Pharm.* 498 (1–2) (2016) 119–129.
- [55] C.H. Evans, V.B. Kraus, L.A. Setton, Progress in intra-articular therapy, *Nat. Rev. Rheumatol.* 10 (1) (2014) 11–22.
- [56] P.A. Simkin, Synovial perfusion and synovial fluid solutes, *Ann. Rheum. Dis.* 54 (5) (1995) 424–428.
- [57] F. Yan, Z. Zhong, Y. Wang, Y. Feng, Z. Mei, H. Li, X. Chen, L. Cai, C. Li, Exosome-based biomimetic nanoparticles targeted to inflamed joints for enhanced treatment of rheumatoid arthritis, *J. Nanobiotechnol.* 18 (1) (2020) 115.
- [58] J. Swierkot, J. Szechinski, Methotrexate in rheumatoid arthritis, *Pharmacol. Rep.* 58 (4) (2006) 473–492.
- [59] V.K. Kolli, P. Abraham, S. Rabi, Methotrexate-induced nitrosative stress may play a critical role in small intestinal damage in the rat, *Arch. Toxicol.* 82 (10) (2008) 763–770.
- [60] B. Zhou, X. Xia, P. Wang, S. Chen, C. Yu, R. Huang, R. Zhang, Y. Wang, L. Lu, F. Yuan, Y. Tian, Y. Fan, X. Zhang, Y. Shu, S. Zhang, D. Bai, L. Wu, H. Xu, L. Yang, Induction and amelioration of methotrexate-induced gastrointestinal toxicity are related to immune response and gut microbiota, *EBioMedicine* 33 (2018) 122–133.
- [61] J. Tu, X. Wang, X. Gong, W. Hong, D. Han, Y. Fang, Y. Guo, W. Wei, Synovial macrophages in rheumatoid arthritis: the past, present, and future, *Mediat. Inflamm.* 2020 (2020) 1583647.
- [62] E.S. Chan, B.N. Cronstein, Molecular action of methotrexate in inflammatory diseases, *Arthritis Res.* 4 (4) (2002) 266–273.
- [63] B.N. Cronstein, T.M. Aune, Methotrexate and its mechanisms of action in inflammatory arthritis, *Nat. Rev. Rheumatol.* 16 (3) (2020) 145–154.